Wind-tunnel interference effects on a 70° delta wing

M. R. Allan, K. J. Badcock, G. N. Barakos and B. E. Richards
Computational Fluid Dynamics Laboratory
Department of Aerospace Engineering
University of Glasgow, UK

ABSTRACT

This paper considers the effects of both wind-tunnel walls and a downstream support structure, on the aerodynamics of a 70° delta wing. A RANS model of the flow was used with the wind-tunnel walls and supports being modelled with inviscid wall boundary conditions. A consistent discretisation of the domain was employed such that grid dependence effects were consistent in all solutions, thus any differences occurring were due to varying boundary conditions (wall and support locations). Comparing solutions from wind-tunnel simulations and simulations with farfield conditions, it has been shown that the presence of tunnel walls moves the vortex breakdown location upstream. It has also been seen that vortex strength, helix angle, and mean incidence also increase, leading to a more upstream breakdown location in wind-tunnels. The secondary separation line was also observed to move outboards. It was observed that for high Reynolds numbers, with a support downstream of the wing, vortex breakdown can be delayed due to blockage effects providing the vortices do not impinge on the support. This was observed to be the case for smaller supports also.

NOMENCLATURE

c_r	root chord
C_p	pressure coefficient
K	kinetic energy of turbulent fluctuations per unit mass
M_∞	freestream Mach number
P_k	limited production of k
P_k^u	unlimited production of k
R	ratio of magnitude of rate of strain and vorticity tensors
S/H	wing span (S) to tunnel height (H)
S/W	wing span (S) to tunnel width (W)
u_τ	friction velocity
U_∞	freestream velocity
X	chordwise distance
y^+	dimensionless, sublayer-scaled, distance, $u_\tau y/\upsilon$
β	closure coefficient
η	spanwise distance/local semi-span
ϕ	helix angle
Γ	circulation
υ	kinematic viscosity
ρ	mass density
ω	specific dissipation rate
ω_x	x component of vorticity vector

1.0 INTRODUCTION

Wind-tunnels are used to test the aerodynamic characteristics of aircraft in the research and development stages. However, the influence of the tunnel walls must be taken into account when considering test results. Historically, wind-tunnel corrections have been based on linear potential flow theory[1]. To obtain good quality and reliable test data, factors relating to wall interference, flow angularity, local variations in velocity, and support interference, must be taken into account. Karou[2] found that for delta wings with aspect ratio equal to one and spanning up to half the tunnel width, classical wall correction techniques can be used to correct flow field and force results up to 30° angle-of-attack (it should be noted that vortex breakdown was unlikely to be present over the wing). Also, for swept wings with a blockage ratio (ratio of model planform area to tunnel cross-sectional area) of less than 0·08, tunnel interference effects can usually be considered negligible[3].

The flow conditions within a wind-tunnel will be different to those a wing would experience in free air. The interactions between the wing and wall flowfields induce longitudinal and lateral variations (streamline curvature and aerodynamic twist respectively) to the freestream, in addition to those attributed to the wing alone. These differences may result in a reduction in the average downwash experienced by the model, a change in the streamline curvature about the model, an alteration to the local angle-of-attack along the span of the

Paper No. 2879. Manuscript received 20 February 2004, accepted 10 August 2004.

model, a change in dynamic pressure about the model due to solid and wake blockage, and in the buoyancy effect due to the axial pressure gradient along the tunnel test section. The magnitude of these effects increases with model size (increasing solid blockage).

Weinberg[4] conducted an experimental investigation into wall effects. He tested two sets of three wings (one set with 60° sweep, and one set with 70° sweep), each wing with a different span size. The experiment was performed in a square water tunnel at a constant flow velocity of 11ms^{-1}. The tunnel size was 45cm × 45cm. He found that for the three wings with 70° sweep, as the wing size was increased (kept at a constant angle-of-attack), vortex breakdown moved downstream. For the three wings with 60° sweep, he found that as the wing span-to-tunnel width ratio increased from 0·175 to 0·35, the wall effects followed the computed trends (i.e. vortex breakdown was shifted downstream with increasing wing size). However, when the wing span-to-tunnel width ratio was increased from 0·35 to 0·7, no significant change was observed. This suggested that effective camber was not the only influence. For both the 60° and the 70° wings, the difference in breakdown location observed from the smallest model to the largest model, was of the order 25% c_r.

Thompson and Nelson[5] investigated experimentally the influence of tunnel walls on a 70° delta wing by testing full, two thirds, and half scale models in a square tunnel (the largest model gave the ratios $S/H = S/W = 0{\cdot}364$). Due to a steady hysteresis effect the wing was tested for a quasi-steady upward and downward stroke. It was found that for the smallest model tested ($S/H = S/W = 0{\cdot}124$) the breakdown location shifted downstream by as much as 15%c_r on both the quasi-steady upstroke and downstroke. For the half scale model and the full scale model, there appeared to be little difference in the breakdown locations. As stated by Thompson and Nelson, this shift downstream as model size is decreased is in contrast to the results of Weinberg[4]. It was noted that Weinberg used a Reynolds number an order of magnitude lower, and a constant velocity, as opposed to keeping the Reynolds number constant (as in the experiments of Thompson and Nelson). It was observed that the vortex suction on the model surface increased with model size.

More recently Pelletier and Nelson[6] studied the effect of tunnel interference on 70° delta wings. Experiments were conducted in a water tunnel with three different sized wings. These low Reynolds number tests agreed with the previous findings of Thompson and Nelson[5] who tested at higher Reynolds number, in that breakdown moved towards the apex with increasing wing size. Pelletier and Nelson used the method of images to explain this effect, concluding that the tunnel walls increased the mean incidence of the wing, thus promoting breakdown.

Verhaagen *et al*[7] performed Euler calculations of the flow over a 76° delta wing inside wind-tunnels of increasing size. The wing span-to-tunnel width ratios considered were 0·292, 0·389, and 0·584 and the test section was octagonal. To model the effect of a secondary separation, a small 'fence' was placed where secondary separation would occur. It was found that decreasing the tunnel size (increasing the wing span-to-tunnel width ratio) increased the suction in the vortices and increased the velocities in the vortex core, due to an increase in circulation with decreasing tunnel size.

Allan *et al*[8] performed Euler simulations of tunnel interference effects on a 65° delta wing in various tunnels for static and pitching cases. It was observed that tunnel side walls were the most influential factor on breakdown location, with roof and floor having little effect. This is due to the fact that the roof and floor of the tunnel are unlikely to have any influence on the effective angle-of-attack of the wing, or on the development of the vortices. It was also noted that in pitching simulations, the tunnel interference effects were strongest on the downstroke, during the vortex reformation.

When considering support interference effects Hummel[9] observed that the presence of an obstacle one chord length downstream of the trailing edge of a delta wing caused vortex breakdown to shift towards the apex by up to 40%c_r. The obstacle considered was unrealistically large (wider than the span of the delta wing), however, this early observation highlighted the possible effects that support structures can have. Recently Taylor *et al*[10] varied the position of various obstacles behind the wing's trailing edge to find the effect support proximity had on vortex breakdown. It was concluded that when an obstacle was placed in the vortex core, breakdown was promoted due to the adverse pressure gradient, which formed in front of the obstacle. As the obstacle was moved away from the vortex core, breakdown was observed to move downstream. It can be expected that the degree of support interference will be dependent on support size, vortex strength and trajectory. Although possibly not considered as support interference, fuselages on delta wing models can effect the breakdown location. Some sting mounted tunnel models have upper surface fuselages to connect the model to the sting. The effect of such fuselages has been considered in a number of investigations, each of which have shown significant variations in breakdown location for a given sweep angle and incidence. See for example Refs (11-13). A possible reason for the variation in the breakdown locations was given by Ericsson[12] in which the effect of the fuselage was described as an induced camber effect. The induced camber effect alters the location of vortex breakdown, either delaying or promoting breakdown depending on the fuselage.

It is the aim of the current work to evaluate the influence of tunnel walls and downstream structures on delta wing aerodynamics. In order to include the influence of the secondary separation a 3D RANS model of the flow is assumed. A particular advantage of CFD for such an investigation is that the various influences can be examined separately, thus the qualitative effect of each component of test facility interference can be evaluated and conclusions drawn.

2.0 COMPUTATIONAL METHOD

All simulations described in this paper were performed using the University of Glasgow PMB3D (Parallel Multi-Block 3D) RANS (Reynolds Averaged Navier-Stokes) solver. A full discussion of the code and turbulence models implemented is given in Ref. 14. PMB3D uses a cell centred finite volume technique to solve the Euler and RANS equations. The diffusive terms are discretised using a central differencing scheme and the convective terms use Roe's scheme with MUSCL interpolation offering third order accuracy. Steady flow calculations proceed in two parts, initially running an explicit scheme to smooth the flow solution, followed by switching to an implicit scheme to obtain faster convergence. The pre-conditioning is based on block incomplete lower-upper (BILU) factorisation and is also decoupled between blocks to help reduce the computational time. The linear system arising at each implicit step is solved using a generalised conjugate gradient (GCG) method. For time-accurate simulations, Jameson's pseudo-time (dual-time stepping) formulation is applied, with the steady state solver used to calculate the flow steady states on each physical time step (discussed fully in Ref. 14).

Since the RANS equations are solved the two equation k-ω turbulence model is used for closure. It is well known that most linear two equation turbulence models over-predict the eddy viscosity within vortex cores, thus causing too much diffusion of vorticity[15]. This weakens the strength of the vortices and can eliminate secondary vortices, especially at low angles of attack where the vortices are already relatively weak. The following modification suggested by Brandsma *et al*[16] was therefore applied to the standard k-ω model of Wilcox[17] to reduce the eddy-viscosity in vortex cores.

$$P_k = \min\{P_k^u, (2{\cdot}0 + 2{\cdot}0\min\{0, r - 1\})\rho\beta^* k\omega\} \quad \ldots (1)$$

Here P_k^u is the unlimited production of k and r is the ratio of the magnitude of the rate-of-strain and vorticity tensors. When k is over predicted in the vortex core, it will be limited to a value relative to the dissipation in that region. This modification was found improve predictions compared with the standard k-ω turbulence model[18].

https://doi.org/10.1017/S0001924000000336 Published online by Cambridge University Press

Table 1
ONERA 70° wing test cases — fully turbulent flow

Tunnel	*S*/*W*	*S*/*H*	M_∞	Re
Farfield	–	–	0·2	$1{\cdot}56 \times 10^6$
ONERA F2	0·49	0·38	0·2	$1{\cdot}56 \times 10^6$
***S*/*W* = 0·63**	0·63	0·38	0·2	$1{\cdot}56 \times 10^6$

3.0 TEST CASES

The subsonic case of a 70° delta wing is considered at 27° angle-of-attack. At this incidence vortex breakdown occurs over the wing. The wing has a root chord length of 950mm, a trailing edge length of 691·5mm, flat upper and lower surfaces, and a leading edge bevel of 15°. The wind-tunnel model had a blunt trailing edge 20mm thick which has been bevelled (15° bevel) in the computational model to simplify the grid generation. Experimental data for this case was obtained by Mitchell[19]. The wing was tested in the ONERA F2 tunnel (situated at Le Fauga-Mauzac Centre, near Toulouse, France) which has a working section of height 1·8m, width 1·4m, and length 5m. It is a subsonic, continuous, closed-return tunnel. The wing was also tested in the ONERA S2Ch tunnel situated at the Chalais-Meudon Centre (ONERA), which is of quasi-circular cross-section with a diameter of 3m and a test section length of 4·93m. The model/tunnel ratios are $S/W = 0{\cdot}49$ and $S/H = 0{\cdot}38$ for the ONERA F2 tunnel, and $S/W = 0{\cdot}23$ and $S/H = 0{\cdot}55$ (taking into account the off tunnel centreline location of wing) for the ONERA S2Ch tunnel. Despite the flow conditions being similar in both tunnels, the mean breakdown locations were closer to the apex in the ONERA F2 tunnel (the smaller of the two) when compared with those measured in the ONERA S2Ch tunnel. This suggests some test facility interference which could be due to either the support structure or tunnel wall interference.

The flow conditions for which extensive experimental data from the ONERA F2 tunnel are available, are an incidence of 27°, Reynolds number of $1{\cdot}56{\times}10^6$, and a freestream velocity of $24 ms^{-1}$ ($M_\infty = 0{\cdot}069$). For these flow conditions, flow visualisation of velocity components, vorticity components, turbulent kinetic energy components and local static pressure are available in various planes. Vortex breakdown locations were also obtained based on where the axial component of velocity becomes negative. In the current work steady state simulations are performed in all cases, with the Reynolds number being matched, however the Mach number is 0·2, compared with the lower Mach number of 0·069 in the experiment. Since the current work is based on a high speed flow solver, a freestream Mach number of 0·2 was used to avoid any possible convergence issues. Transition was observed to occur at around 40%c_r in experiment, however the CFD simulations assume a fully turbulent flow. As will be described the fully turbulent flow assumption will influence the validation of the results. However, the tunnel interference will mainly be dependent on vortex strength, thus the fully turbulent assumption is unlikely to influence the trends observed (the leading edge separation location is fixed due to the sharp leading edge and breakdown is known to be independent of Reynolds number[20]).

Three boundaries have been chosen. The first has the wing in free air (farfield conditions), the second represents the ONERA F2 tunnel, and the third the ONERA F2 tunnel side walls brought closer to the wing (increasing the *S*/*W* ratio). Full details of these configurations as well as flow parameters can be found in Table 1.

To assess the effects of downstream structures in the tunnel a vertical (generic) structure was placed in the centre of the ONERA F2 tunnel, downstream of the wing. Since supports in dynamic testing tend to be fairly large (driving mechanisms must also be housed) a thick cross-sectional area for the support was chosen. The generic structure considered is a cylinder with a straight taper in the downstream direction. Figure 1 shows the support structure and its placement within the ONERA F2 tunnel. To avoid grid generation complications the mounting attaching the wing to the vertical structure is omitted (it may be expected that there is further interference from this mounting). The downstream structure (shown in Fig. 2 with dimensions) gives a frontal area blockage of around 12%.

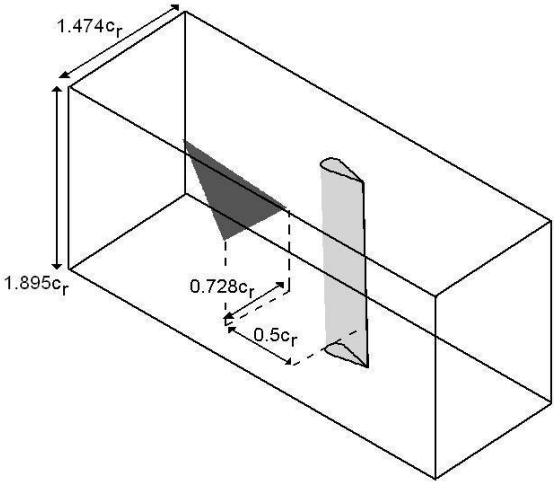

Figure 1. ONERA F2 tunnel setup with downstream structure.

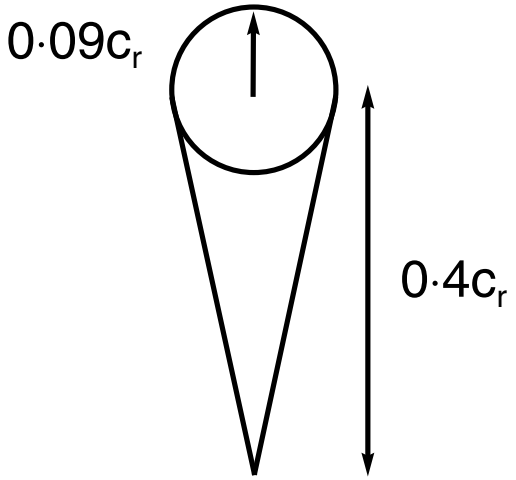

Figure 2. Geometry of downstream support structure (plan view).

The support structure was placed at two downstream locations in the ONERA F2 tunnel, at $0{\cdot}5c_r$ and $1c_r$ from the trailing edge of the wing. The mesh over the wing is identical to that for the ONERA F2 tunnel without downstream structures. Therefore there is no change in grid resolution in the vortical region above the wing. The ONERA F2 tunnel mesh was altered downstream of the wing to allow the presence of the structure.

In all cases considered the tunnel walls and downstream support structures have been modelled with inviscid wall boundary conditions. Eliminating the tunnel wall boundary layers reduces grid sizes, however, a consequence of this is that the favourable pressure gradient within the test section (due to tunnel wall boundary-layer

https://doi.org/10.1017/S0001924000000336 Published online by Cambridge University Press

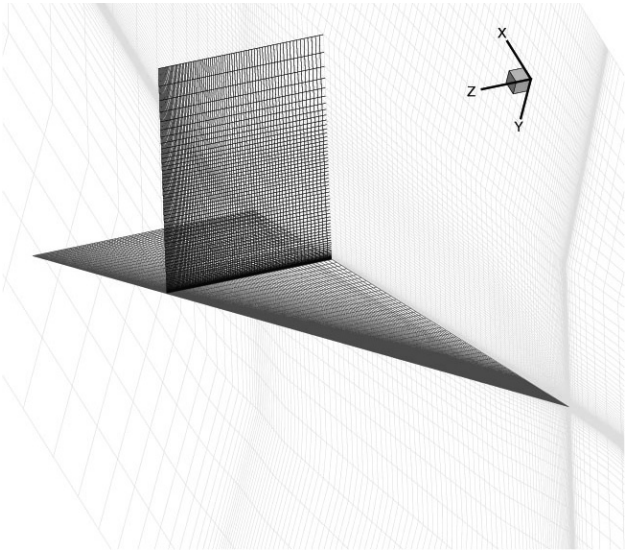

Figure 3. View of ONERA F2 tunnel mesh.

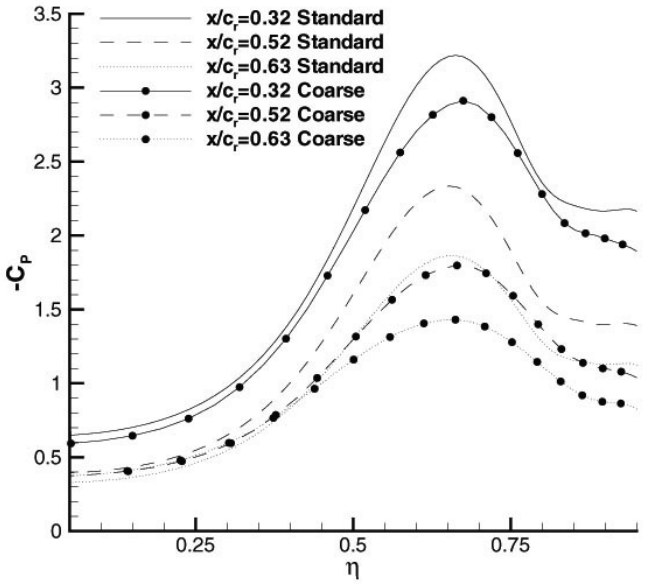

Figure 4. Dependency of upper surface pressure distribution with grid refinement.

Table 2
Viscous grid dimensions

Test case	Normal to upper surface	Total
Farfield	117	3,969,810
ONERA F2	103	2,904,660
***S/W* = 0·63**	103	2,664,090

growth) is not modelled. However, it is expected that the lack of tunnel wall boundary layers in the present simulations will not effect the trends observed, which are mainly due to wall induced velocities.

4.0 COMPUTATIONAL GRIDS

The ONERA 70° wing inside the ONERA F2 tunnel is considered. A depiction of the grid around the ONERA 70° wing is given in Fig. 3. The mesh is of *H-H* topology with only half the wing modelled at 27° angle-of-attack (a symmetry condition is applied at the wing centre plane). The tunnel grids have been extracted from the 'farfield' grid by removing outer blocks, thus the mesh resolution over the wing is identical in each case. This methodology ensures that any differences are due only to changes in boundary conditions (such as locations of tunnel walls and support structures). The first cell height normal to the wing surface is $10^{-6}c_r$. This yields an average y^+ value of less that 1·0. The mesh sizes are given in Table 2. All grids had 99 points streamwise and 79 points spanwise over the wing.

5.0 VERIFICATION AND VALIDATION

The solutions described in this paper have been previously validated[18]. Therefore only a brief discussion is presented here. Due to the computational requirements for predicting time accurately the unsteady nature of the breakdown region of a leading edge vortex, in the current work steady state simulations are considered. As such the unsteady features (such as the helical mode instability) associated with vortex breakdown are not simulated. It is assumed that the steady state results represent a time-averaged solution of the unsteady flow, however this should be confirmed with time-accurate results. In order to validate and assess the predictions with the modified k-ω turbulence model, the ONERA 70° wing inside the ONERA F2 tunnel is considered. In order to attempt to verify the accuracy of the solutions, a limited grid dependency study has been conducted. Due to the high computational power requirements to solve the flow with the fine grid, only a comparison with the coarse grid solution is presented. The 'coarse' grid is created by extracting a level in each direction from the standard grid. The upper surface pressure distributions are given in Fig. 4. The breakdown locations from the coarse and standard grids are 59·6%c_r and 64·7%c_r respectively. Clearly as we go from the coarse to standard grids the suction peaks increase in strength and vortex breakdown moves downstream.

Flow visualisation of the solutions indicates that a grid refinement increases the core properties (higher suction, higher axial velocities, higher vorticity) and increases turbulence levels within the vortex. Clearly as breakdown is delayed going from the coarse to the standard grid, the increase in the core properties is dominant over the dissipation of kinetic energy in the vortex, allowing the core flow to negotiate the adverse pressure gradient a little further. It should be noted that Visbal and Gordnier[21] observed for simulations on a 75° delta wing at 25° angle-of-attack, with Reynolds number equal to 2×10^6, and freestream Mach number of 0·2, that on a coarse grid (*H-H* topology) vortex breakdown was located upstream to that computed on a finer grid. Since the grids used for the tunnel calculations have been extracted from a common farfield grid, the grid dependency of each solution will be similar. As such, despite the fact that further refinement of the vortices is required (which is not currently feasible due to computing limitations), the grid dependency is equal for all cases, and therefore solution to solution comparisons for tunnel effects is valid.

In all solutions the mean flow residual converged at least six orders of magnitude. If we examine the upper surface pressure distributions at the chordwise stations of x/c_r = 0·32, 0·52, and 0·63 (Fig. 5), we see good agreement between the experimental and predicted flow at the chordwise location of x/c_r = 0·32. We also see that the main features of a primary and secondary vortex are evident at all chordwise stations. However, the variation in the strength of the vortex footprint in the chordwise direction reduces faster in the CFD solutions in comparison to experiment (the suction peaks at x/c_r = 0·53 and 0·63 are considerably lower than in experiment). This may be due to the vertical position of the vortex being poorly predicted

https://doi.org/10.1017/S0001924000000336 Published online by Cambridge University Press

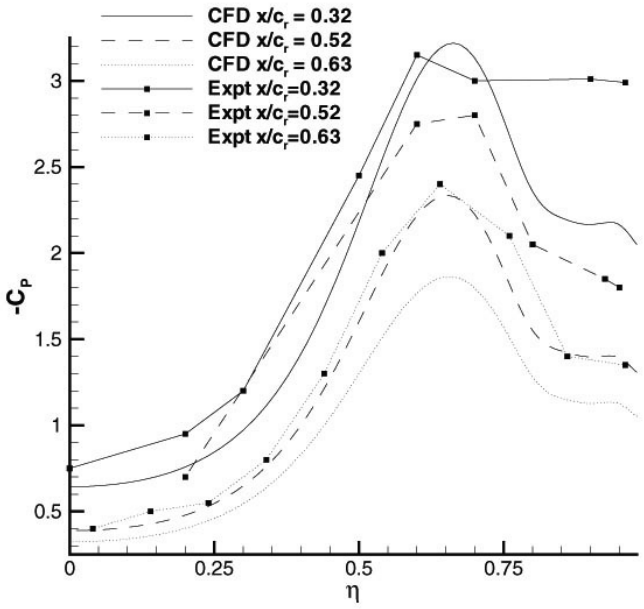

Figure 5. Comparison of upper surface pressure distribution with experiment.

(due to the laminar/turbulent transition in experiment varying the position of the vortex core), or that the grid resolution is insufficient. The suction levels near the apex (where the flow is highly resolved) compare well with experiment, despite the strength of the secondary vortex being under-predicted (most likely due to the turbulent flow assumption in the CFD solutions). Given that in experiment the flow is laminar up to 40%c_r, and that the secondary separation moves outboard on transition[19], the secondary vortices in the CFD solutions are likely to be larger than in experiment downstream of the transition point. This will have the effect of shifting the primary vortex off the surface, reducing the suction peak in the chordwise direction.

Although not presented, the distribution of the core axial velocities was also compared with experiment. It was observed that the peak core velocities were around 2·5 times freestream, compared with 3·5 times freestream in experiment. Such deficits in core velocities have been observed by others[22,23] and may be attributed to spatial schemes or the very high grid density requirements to model the vortex core. The core axial vorticity levels were also compared with experiment, as were the helix angles, and good agreement was found. This indicates that the strength of the vortices is well predicted.

6.0 RESULTS

In order to obtain the breakdown locations above the wing, the location at which the axial component of velocity becomes zero was taken as the breakdown point. This is consistent with the method used in experiment[19]. To achieve this, a vertical slice through the vortex core was taken and the point where the axial velocity becomes zero was measured. The breakdown locations for the three test cases without support structures are given in Table 3.

The promotion of vortex breakdown is comparable in magnitude (though a little lower) to the promotion of vortex breakdown seen experimentally when going from the larger ONERA S2Ch tunnel to the smaller ONERA F2 tunnel. It should be kept in mind that support effects have been omitted in the CFD solutions. As in Euler simulations[8] increasing the *S*/*W* ratio has the effect of promoting vortex breakdown.

Table 3
Summary of steady breakdown locations for ONERA 70° wing at 27° angle-of-attack

TUNNEL	*S*/*W*	*S*/*H*	Breakdown location
Farfield	–	–	68·8%c_r
ONERA F2	0·49	0·38	64·7%c_r
***S*/*W* = 0·63**	0·63	0·38	60·3%c_r
Experiment	0·49	0·38	65±5%c_r
ONERA F2			
Experiment	0·23	0·55	≅72%c_r
ONERA S2Ch			

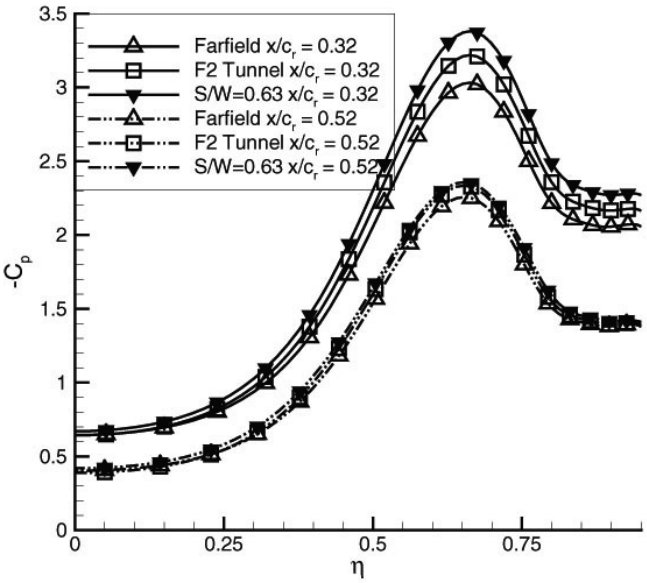

Figure 6. Comparison of upper surface pressure distributions, $x/c_r = 0{\cdot}32$ and $x/c_r = 0{\cdot}52$.

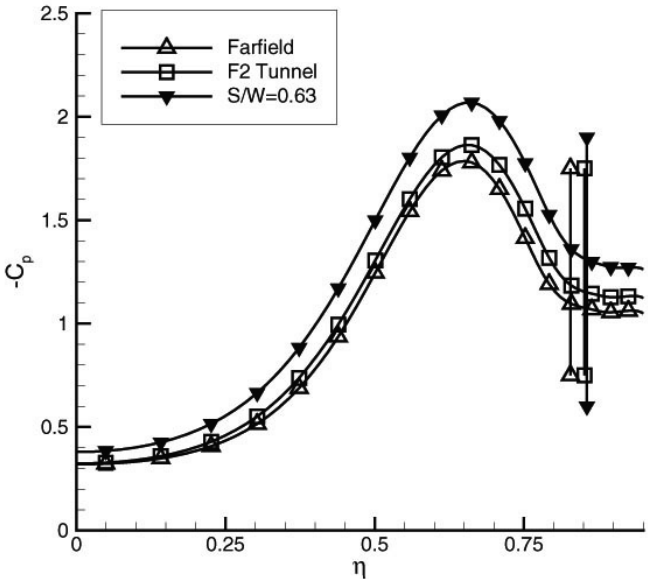

Figure 7. Comparison of upper surface pressure distributions and secondary separation locations, $x/c_r = 0{\cdot}63$.

Figures 6 and 7 show thze spanwise surface pressure distributions at the chordwise locations of $x/c_r = 0{\cdot}32$, $x/c_r = 0{\cdot}52$, and $x/c_r = 0{\cdot}63$. Also shown in Fig. 7 are the secondary separation locations at $x/c_r = 0{\cdot}63$ (taken to be where the spanwise shear stress component

https://doi.org/10.1017/S0001924000000336 Published online by Cambridge University Press

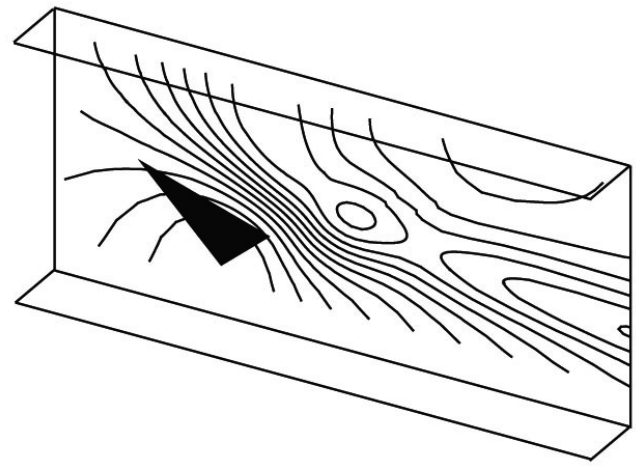

(a) ONERA F2 tunnel.

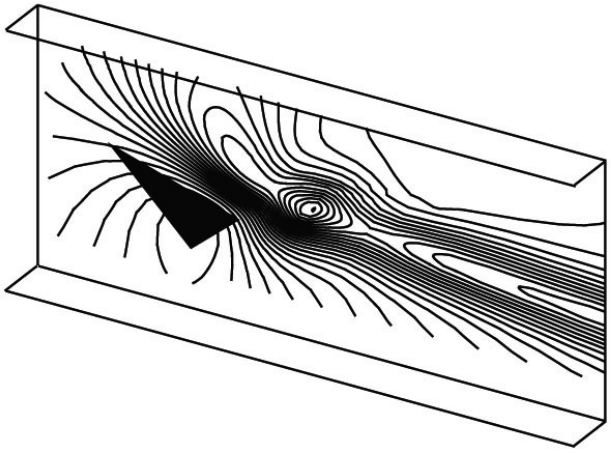

(b) $S/W = 0{\cdot}63$ tunnel

Figure 8. Steady flow tunnel wall pressure distributions.

changes sign), which are indicated by vertical lines for all three cases. It can be seen that the presence of wind-tunnel walls causes the secondary separation line to move outboard (i.e. secondary separation is delayed). The delay in secondary separation is also observed at the more upstream chordwise locations, however the variations are less apparent. The delay in secondary separation will be discussed later. Clearly when the flow is confined by the ONERA F2 tunnel, the primary suction peak increases, and increases further as the side wall proximity becomes nearer the wing (the $S/W = 0{\cdot}63$ tunnel). It can also be seen that the secondary vortex increases in strength, almost equally in comparison to the primary suction peak, with increasing S/W.

The tunnel wall pressure distributions on the ONERA F2 and the $S/W = 0{\cdot}63$ tunnels are shown in Fig. 8. The contour limits for the pressure coefficient plots are $-0{\cdot}2 \le C_p \le 0{\cdot}2$. It can be see that there is a strong vortical flow pattern on the side walls, which extends down the tunnel despite vortex breakdown having occurred (the persistence of vortical flow despite breakdown occurring was also observed during experiments). The flow patterns appear similar for the ONERA F2 tunnel and the $S/W = 0{\cdot}63$ tunnel, however the strength of the pressure variations increases with increasing S/W ratio. Given the pressure gradients on the tunnel side walls, it is clear there is a significant amount of interference induced by the side walls.

In order to assess the adverse pressure gradient experienced by the vortex core, the pressure distribution along the vortex core in each

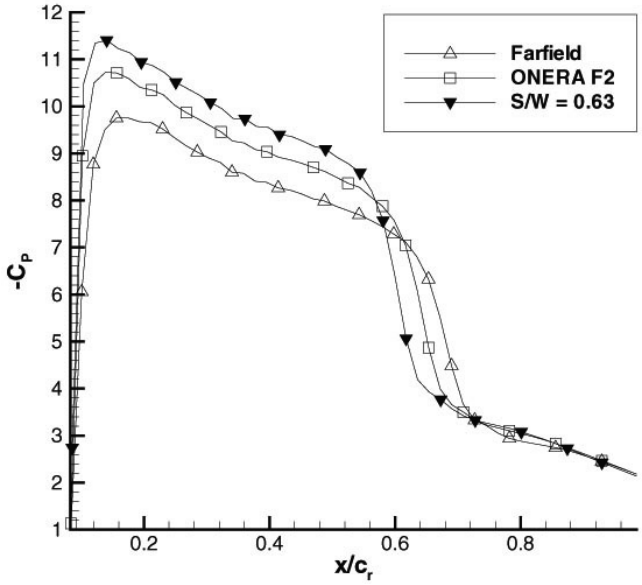

Figure 9. Pressure distributions along vortex cores.

tunnel is compared in Fig. 9. Visbal[24] found that vortex breakdown was heavily dependent on the pressure gradient experienced by the vortex core. As the wing is placed in a tunnel the suction in the vortex core prior to breakdown increases. This indicates that when the vortices are placed within wind-tunnels, they become stronger than those in farfield conditions. With this additional suction the adverse pressure gradient experienced by the core flow increases, thus vortex breakdown is expected to be promoted. This agrees qualitatively with the results of Visbal.

The flow angle (the angle at which the freestream is turned up due to the presence of the wing and side walls) variation in the streamwise direction can be seen in Fig. 10. Both tunnels increase the flow angle ahead of the wing in comparison to the farfield solution, and also increase the rate at which the flow angle increases along the wing. There are two possible effects present, an increase in the mean effective incidence and induced camber. Both these effects increase with increasing S/W. Since breakdown has moved towards the apex it is expected that the increase in the mean effective incidence is the dominant effect.

Figure 11 shows the helix angle variation through the middle (horizontal line) of the vortex core at the chordwise location of $x/c_r = 0{\cdot}52$. At this chordwise location the vortex is unburst in all solutions. The experimental helix angle obtained in the ONERA F2 tunnel[19] is also given for comparison. As the tunnel walls get closer to the wing it can be seen that the helix angle increases (the turns of the vortex tighten), which can cause a promotion of vortex breakdown[25]. This is due to the side wall inducing additional vertical velocity components, which increases the mean effective incidence of the wing. The tightening of the vortex also increases the cross flow momentum. Given that the adverse pressure gradient experienced by the wing boundary layer is unchanged as it passes from beneath the primary vortex core to the secondary separation region (since the secondary suction also increases with the primary suction), the likely cause of the predicted delay in secondary separation due to tunnel walls, is an increase in cross flow momentum due to the tighter windings of the vortex. It can also be seen that the location at which the helix angle changes sign (as we pass through the vortex core) does not appear to move significantly with increasing S/W ratio, indicating the vortex core does not move spanwise significantly at this chordwise location.

https://doi.org/10.1017/S0001924000000336 Published online by Cambridge University Press

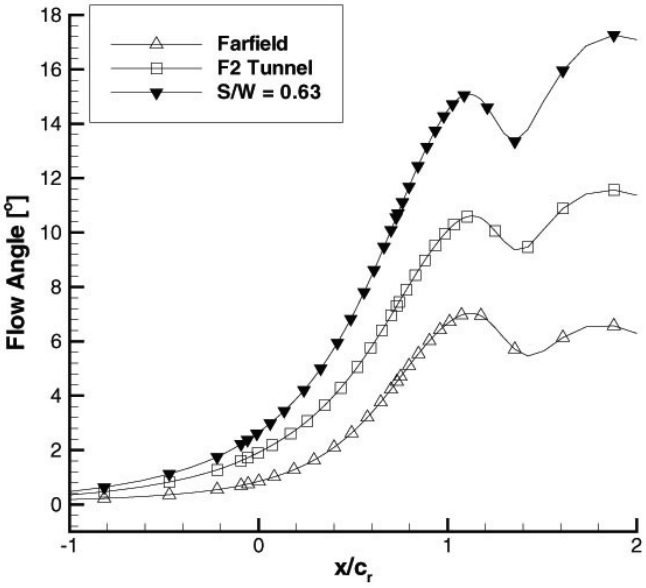

Figure 10. Flow angles at 1·5 wing span lengths from wing.

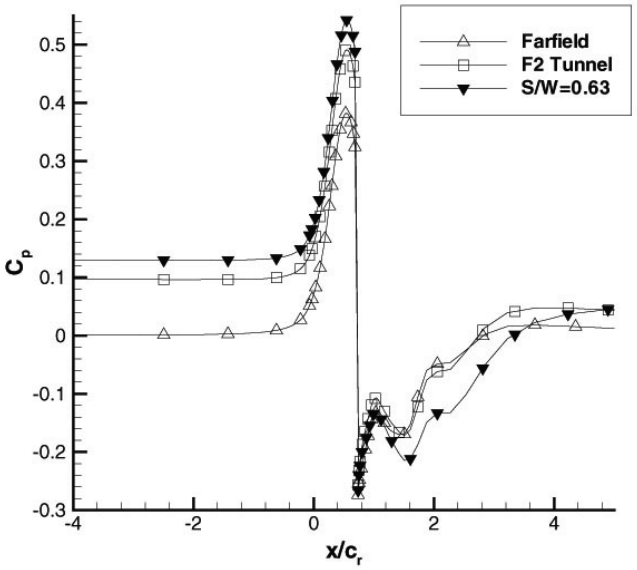

Figure 12. Tunnel centreline pressure distributions.

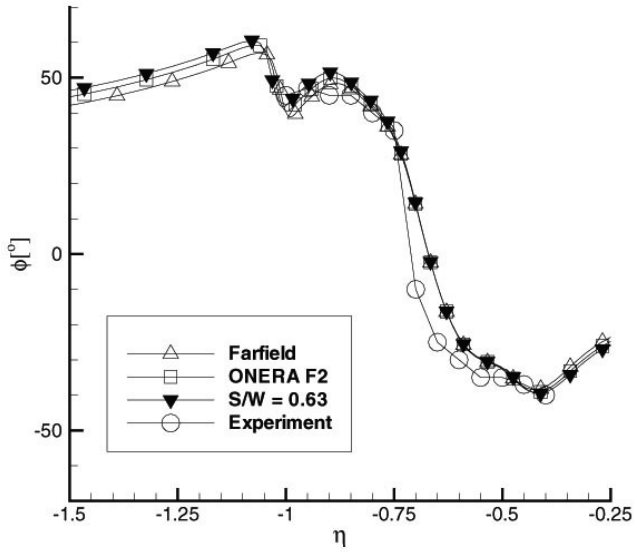

Figure 11. Comparison of helix angles through vortex cores at $x/c_r = 0{\cdot}52$.

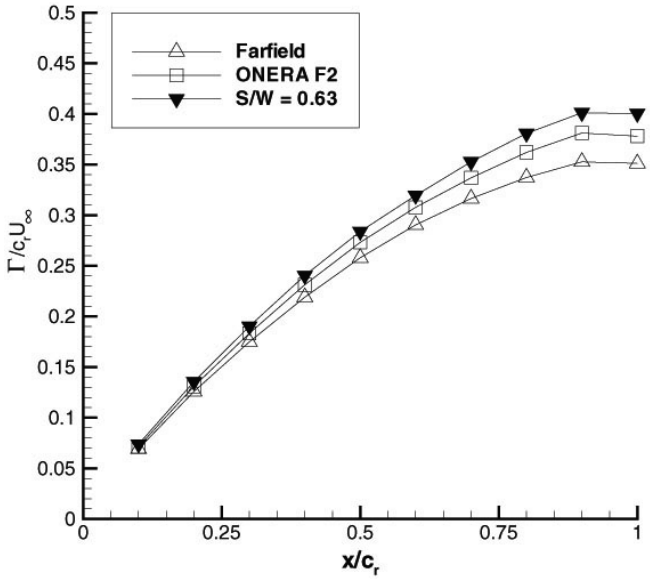

Figure 13. Comparison of circulation distributions.

The static pressure distribution along the centreline of the tunnels can be seen in Fig. 12. As the centreline passes through the wing the switch from the pressure side to the suction side can be seen as a jump in the curve at approximately $x/c_r = 0{\cdot}75$. It is evident that as the tunnel size decreases the static pressure beneath the wing increases (as expected due to increasing frontal area blockage). The suction over the wing upper surface also increases with decreasing tunnel size. Figure 12 also indicates that the broken down vortex system is lifted into the centre of the tunnels. If the vortex structure is lifted, we can expect a relative decrease in local static pressure along the tunnel centreline. Behind the wing the tunnel pressure distributions are slightly above that of the farfield solution. However, it should be recalled that there are two influences on the tunnel static pressure in this region, the blockage effect increasing the static pressure within the tunnel and the vortex lifting, which decreases the pressure in this region. Deducting the blockage effect we see that there is a relative decrease in static pressure indicating the vortices have lifted closer to the centreline in the tunnel simulations. The displacement of the vortices was confirmed with flow visualisations.

The chordwise variation in circulation along the vortices for each case is given in Fig. 13. The circulation was obtained by integrating the ω_x component of the vorticity vector over ten chordwise slices. The oppositely signed secondary separation region was omitted (which would have the effect of lowering the circulation values). From the apex to around the midchord position it can be seen there is a relatively linear growth in circulation in the chordwise direction, after which the rate of growth in circulation decreases[26]. Despite vortex breakdown occurring the circulation continues to increase in the chordwise direction[27], eventually becoming near constant as the trailing edge is reached. The integrations were performed over an entire extracted plane, thus it would appear rather than there being a

https://doi.org/10.1017/S0001924000000336 Published online by Cambridge University Press

Table 4
Vortex breakdown locations with and without downstream support structures

Incidence	Support location	Breakdown location
27°	0·5 c_r	81·0%c_r
27°	1 c_r	65·9%c_r
27°	NONE	64·7%c_r

loss in the ω_x component of vorticity, it is dispersed throughout the vortex. If the integration region is not large enough to encompass this dispersion, it may appear that there is a loss in circulation. The circulation curves further indicate that as the wing is placed in wind-tunnels the vortices become stronger, strengthening with increasing S/W ratio.

7.0 SUPPORT STRUCTURE EFFECTS

The predicted breakdown locations when downstream support structures are added, are given in Table 4. Again the breakdown locations have been taken where the axial velocity equals zero.

It can be seen that when the support structure is located 1c_r downstream of the wing trailing edge, there appears to be only a small influence on the breakdown location, with breakdown being delayed slightly in comparison to the case without support structures. Since the vertical support used in the experiments of Mitchell[19] was placed around 2c_r from the trailing edge of the wing, it can be concluded that its interference effect on the experimental breakdown location is likely to be minimal. As the support structure gets closer to the trailing edge of the wing (at 0·5c_r from the trailing edge) it can be seen that the vortex breakdown location shifts back towards the trailing edge by around 16·3%c_r. This is in contrast to what may be considered as the common understanding that downstream structures induce vortex breakdown due to pressure disturbances propagating upstream.

To determine the reason why the downstream structure delays vortex breakdown, the structure of the vortices prior to breakdown was examined. The flow angles (the angle at which the freestream is deflected due to the presence of the wing) were examined and it was observed that there is little change due to supports being placed in the tunnel. The flow angles are therefore only being altered by the proximity of the vortices to the side wall (which induces vertical velocity components increasing the mean incidence of the wing). Indeed provided the vortices do not increase in strength as a result of support interference, the flow angles should remain unchanged. The surface pressure distributions above the wing at x/c_r = 0·32, 0·52, and 0·63 were also examined and again there was little difference is solutions with and without support structures, both in core location and suction peaks. The axial vorticity distributions and chordwise distribution of circulation were finally examined, and it was concluded that prior to breakdown, the support structures have no influence on the vortex structure.

Figures 14 and 15 shows the pressure coefficient distribution along a horizontal plane at the midpoint between the tunnel roof and floor for each support location. The contour levels plotted range from $-2{\cdot}7 \le C_p \le 0{\cdot}6$ in both figures. The flow direction is from top to bottom and the intersection of the horizontal plane with the wing is clearly seen upstream of the support structure. For both downstream structure locations the vortical flow negotiates the support as opposed to impinging on it (as in the experiments of Taylor *et al*[10,28]). Since the mean effective incidence of the wing and strength of the vortices is unaltered prior to vortex breakdown, the only explanation for the delay in vortex breakdown is a change in the pressure gradient in the tunnel. It is well understood that vortex breakdown is sensitive to external pressure gradients[29].

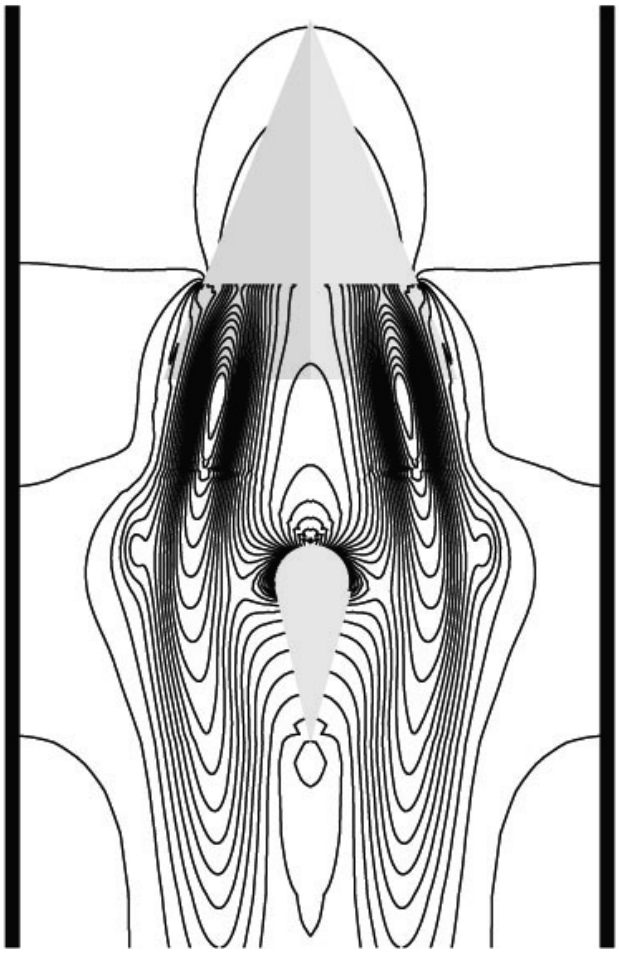

Figure 14. Pressure distribution along a horizontal plane, support 0·5c_r from wing trailing edge.

Examination of the tunnel axial pressure gradients indicated that as the support becomes near the wing, a local (to the wing) favourable pressure gradient develops. It should be noted that the pressure gradient at the side wall was examined, not the pressure gradient along the centreline of the tunnel which would incorporate an adverse pressure gradient as the support is approached. Since the vortices do not impinge on the support they will not experience this adverse pressure gradient, therefore the pressure gradient at the side wall is more indicative of the pressure gradient experienced by the vortices. The favourable pressure gradient is due to an acceleration of the flow as it negotiates the support, thus reducing the local static pressure around the support. To have an effect on vortex breakdown the favourable pressure gradient must be local with respect to the vortices, and so when the support is placed 1c_r from the wing, the favourable pressure gradient around the support has a smaller effect.

From the previous discussion it is clear that downstream support structures have the sole effect of altering the pressure gradients within the tunnel. There is little or no change to the vortex structure prior to vortex breakdown. Clearly the shape and size of the support considered in this study alters the pressure gradients in the tunnels due to blockage effects. The acceleration of the flow around the support causes a favourable pressure gradient to form, and if this pressure gradient is local with respect to the vortices, breakdown is delayed. However there is also a stagnation region ahead of the

https://doi.org/10.1017/S0001924000000336 Published online by Cambridge University Press

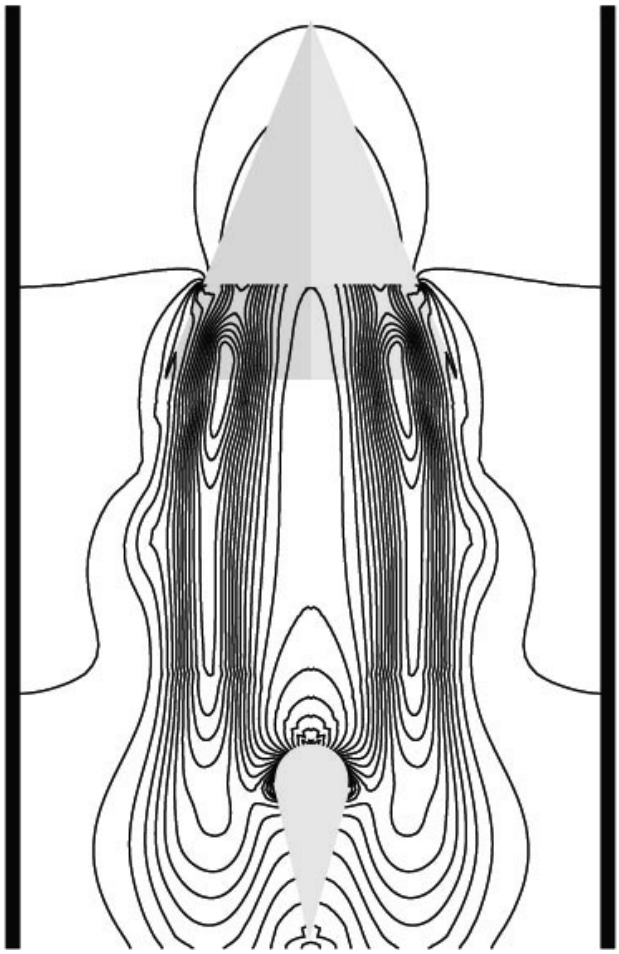

Figure 15. Pressure distribution along a horizontal plane, support $1c_r$ from wing trailing edge.

support thus it is possible that if the blockage effect is lowered, the stagnation effect may become dominant and breakdown will be promoted. To assess any possibility of this a narrower support was placed at $0{\cdot}5c_r$ from the trailing edge of the wing. The geometry is identical to that described in Fig. 2, however the radius of the cylindrical section was reduced from $0{\cdot}09c_r$ to $0{\cdot}045c_r$. This effectively halves the support frontal area blockage from approximately 12% to 6%. The breakdown was observed to shift from $64{\cdot}7\%c_r$ to $73{\cdot}8\%c_r$. Clearly despite the blockage being reduced the previous discussion applies to thinner vertical support structures. Therefore as long as the vortex cores negotiate the support structure, breakdown can be delayed. This seems to be the case for 'streamlined' tunnel-centred support structures at high Reynolds number. The effect of the favourable pressure gradient at low Reynolds number is likely to be lower.

8.0 CONCLUSIONS

A CFD investigation of wind-tunnel interference effects on a 70° delta wing has been conducted. The vortical flow predictions were initially verified and validated, and then used to analyse the various effects of test facility interference. From the current work the following has been observed:

- The presence of wind-tunnel side walls promotes vortex breakdown.
- The amount of upwash generated (and therefore the mean effective incidence of the wing) increases as the model span to tunnel width ratio increases.
- Despite the possible presence of an induced camber effect, since breakdown is promoted it is apparent that the increase in mean effective incidence is the dominant factor.
- The helix angle of the vortices increases due to the side wall induced upwash. This is known to promote vortex breakdown.
- The secondary separation location moves towards the leading edge when the wing is placed inside wind-tunnels. This is due to an increase in cross flow momentum as the helix angle increases.
- Downstream support structures have no effect on the flow structure prior to vortex breakdown.
- The effect of downstream support structures is likely to be dependent on whether or not the core flow impinges on the structure.
- With the support shape and flow conditions considered, vortex breakdown was delayed due to blockage effects.
- Such a result is likely to correspond to high Reynolds number flows, and will therefore be Reynolds number dependent. This result should be confirmed experimentally with particular attention being paid to Reynolds number effects.

Since turbulence modelling plays a significant role in the prediction of vortical flows, the work presented should be considered a qualitative assessment of tunnel interference effects. In order to improve the accuracy and validate further the predictions, time-accurate simulations and more advanced turbulence modelling (such as detached eddy simulation) should be employed.

ACKNOWLEDGEMENTS

The authors wish to thank the participants of the RTO AVT-080 Task Group on 'Vortex breakdown over slender wings' for many enlightening discussions. The financial support from QinetiQ (formerly DERA Bedford) is gratefully acknowledged.

REFERENCES

1. GARNER, H.C. and ROGERS, E.W.E. Subsonic wind-tunnel wall corrections, AGARDograph 109, 1966.
2. KAROU, A. Separated vortex flow over slender wings between side walls — theoretical and experimental investigation, 1980, Report LR-300, Dept of Aerospace Engineering, Delft University of Technology.
3. Engineering Sciences Data Unit, Blockage corrections for bluff bodies in confined flows, 1980, Item 80024, London.
4. WEINBERG, Z. Effect of tunnel walls on vortex breakdown location over delta wings, *AIAA J*, June 1992, **30**, (6).
5. THOMPSON, S.A. and NELSON, R.C. wind-tunnel blockage effects on slender wings undergoing large amplitude motions, AIAA-92-3926, July 1992.
6. PELLETIER, A. and NELSON, R.C. Factors influencing vortex breakdown over 70° delta wings, 1995, AIAA-95-3469-CP.
7. VERHAAGEN, N.G., HOUTMAN, E.M. and VERHELST, J.M. A study of wall effect on the flow over a delta wing, 1996, AIAA-96-2389.
8. ALLAN, M.R., BADCOCK, K.J. and RICHARDS, B.E. A CFD Investigation of wind-tunnel wall influences on pitching delta wings, June 2002, AIAA-2002-2938.
9. HUMMEL, D. Untersuchungenüber das Aufplatzen der Wirbel an schlanken Delta Flügeln, Zeitschrift für Flugwissenschaften, 1965, **13**, (5), pp 158-168.
10. TAYLOR, G., GURSUL, I. and GREENWELL, D. Static hysteresis of vortex breakdown due to support interference, 2001, AIAA 2001-2452.
11. STRAKA, W.A. Effect of fuselage on delta wing vortex breakdown, *J Aircr*, 1994, **31**, (4), pp 1002-1005.
12. ERICSSON, L.E. Effect of fuselage geometry on delta-wing vortex breakdown, *J Aircr*, November-December 1998, **35**, (6).
13. ERICSSON, L.E. Further analysis of fuselage effects on delta wing aerodynamics, January 2000, AIAA 2000-0891.

https://doi.org/10.1017/S0001924000000336 Published online by Cambridge University Press